Accepted Manuscript

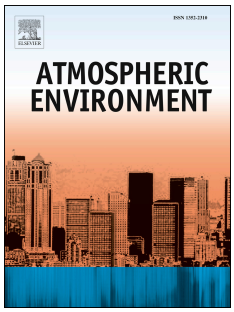

Observational evidence of cloud processes contributing to daytime elevated nitrate in an urban atmosphere

Jun Tao, Zhisheng Zhang, Haobo Tan, Leiming Zhang, Yunfei Wu, Jiaren Sun, Huizhen Che, Junji Cao, Peng Cheng, Laiguo Chen, Renjian Zhang

PII: S1352-2310(18)30344-3

DOI: 10.1016/j.atmosenv.2018.05.040

Reference: AEA 16031

To appear in: *Atmospheric Environment*

Received Date: 8 December 2017

Revised Date: 17 May 2018

Accepted Date: 22 May 2018

Please cite this article as: Tao, J., Zhang, Z., Tan, H., Zhang, L., Wu, Y., Sun, J., Che, H., Cao, J., Cheng, P., Chen, L., Zhang, R., Observational evidence of cloud processes contributing to daytime elevated nitrate in an urban atmosphere, *Atmospheric Environment* (2018), doi: 10.1016/j.atmosenv.2018.05.040.

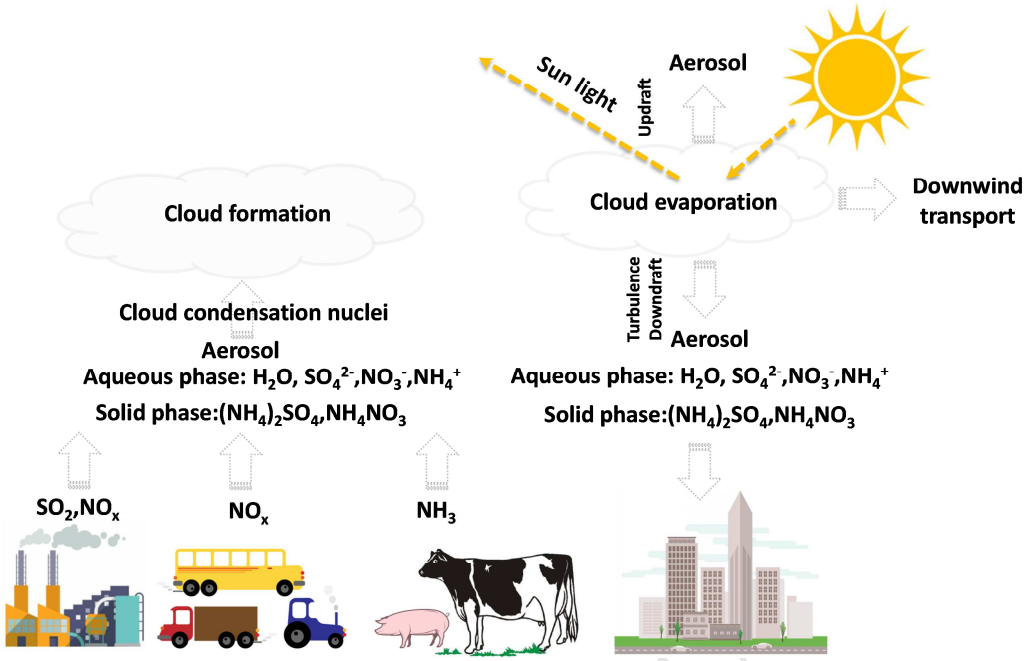

Observational evidence of cloud processes contributing to daytime elevated nitrate in an urban atmosphere

Jun Tao[1*], Zhisheng Zhang[1], Haobo Tan[2], Leiming Zhang[3,*], Yunfei Wu[4], Jiaren Sun[1], Huizhen Che[5], Junji Cao[6], Peng Cheng[7], Laiguo Chen[1], Renjian Zhang[4]

[1]South China Institute of Environmental Sciences, Ministry of Ecology and Environment, Guangzhou, China

[2]Key Laboratory of Regional Numerical Weather Prediction, Institute of Tropical and Marine Meteorology, China Meteorological Administration, Guangzhou, China

[3]Air Quality Research Division, Science and Technology Branch, Environment and Climate Change Canada, Toronto, Canada

[4]RCE-TEA, Institute of Atmospheric Physics, Chinese Academy of Sciences, Beijing, China

[5]Institute of Atmospheric Composition, Chinese Academy of Meteorological Sciences, China Meteorological Administration, Beijing, China

[6]Key Laboratory of Aerosol Chemistry and Physics, Institute of Earth Environment, Chinese Academy of Sciences, Xi'an, China

[7]Institute of Mass Spectrometer and Atmospheric Environment, Jinan University, Guangzhou, China

Correspondence to: J. Tao (taojun@scies.org) or L. Zhang (leiming.zhang@canada.ca)

Abstract. Nitrate has become the most important hydrophilic chemical component in $PM_{2.5}$ during serious air pollution periods in urban areas of the Pearl River Delta (PRD) region of south China, but there is a lack of fully understanding of its formation mechanisms and controlling factors, especially during daytime nitrate episodes. To fill the knowledge gap, water-soluble inorganic ions in $PM_{2.5}$ and trace gases including SO_2, HNO_3, NH_3, NOx and O_3, particle size distribution, vertical profile of aerosol backscatter density, and ground-level and vertical profiles of key meteorological variables were simultaneously measured at high time resolution in urban Guangzhou of the PRD. The remarkably enhanced nitrate mass concentrations observed at the surface-level during daytime were identified to be caused by strong boundary-layer turbulent mixing of residual aerosols produced from evaporation of low-level shallow stratocumulus clouds. This finding may have important implications on the sources of secondary inorganic aerosols in this and other similar cloudy regions.

Key words: nitrate episode; aerosol size distribution; cloud processed aerosols; boundary-layer mixing

1. Introduction

Nitrate constitutes a substantial fraction of fine particles and thus has significant impacts on air quality and climate related issues such as acid deposition, reduced visibility, radiative forcing, and aerosol-cloud interaction (*Shindell et al.*, 2009; *Tao et al.*, 2017; *Watson*, 2002; *Zhang et al.*, 2007). Nitrate is one of the most important pathways removing nitrogen oxides (NOx), which are the major primary emissions produced from fossil fuel combustion processes, soil, biomass burning and lighting, from the atmosphere (*Andreae & Merlet*, 2001; *Davidson & Kingerlee*, 1997; *Hudman et al.*, 2007; *Richter et al.*, 2005). In the atmosphere, NOx can be converted into nitrate in two chemical mechanisms (*Zhang et al.*, 2015). The first one is through the oxidation of nitrogen dioxide (NO_2) to $HNO_{3(g)}$ with the media of hydroxyl radical ($OH\cdot$) during daytime. The second one is through the chemical reaction between NO_2 and O_3 to form nitrate radical (NO_3), which further reacts with NO_2 to form dinitrogen pentoxide (N_2O_5) during nighttime. $HNO_{3(g)}$ and (N_2O_5) can then be easily converted to particle nitrate through gas- or aqueous-phase reactions.

Nitrate episodes have been mostly observed during the nighttime and have been found to be strongly related to high NO_2, NH_3, O_3 and ambient relative humidity (*Dall'Osto et al.*, 2009; *Pathak et al.*, 2011; *Wang et al.*, 2009; *Wen et al.*, 2015). N_2O_5 has not been directly measured in these studies, but has been suspected to be the main cause of the nocturnal nitrate episodes through hydrolysis process. A recent study showed higher N_2O_5 concentrations during pollution episodes in an urban environment in Beijing, demonstrating the important contribution of nighttime nitrate formation to aerosol loading (*Wang et al.*, 2017). However, the dominant formation mechanisms for nitrate during daytime remain controversial. Besides the oxidation of NO_2 via OH (*Alexander et al.*, 2009; *Seinfeld & Pandis*, 2012), the hydrolysis of N_2O_5

might also be important according to a multiphase chemistry box-model study in the PRD region (*Xue et al.*, 2014). However, N_2O_5 is prone to dissociate back to NO_3 and NO_2 during daytime due to its photolysis and thermal decomposition properties (*Seinfeld & Pandis*, 2012; *Wängberg et al.*, 1997), and thus extremely low concentrations of NO_3 and N_2O_5 have been commonly observed (*Chang et al.*, 2011; *Stutz et al.*, 2010).

Daytime nitrate episodes have been observed in Hong Kong of the PRD by the same research group, but different interpretations of formation mechanisms have been provided (*Griffith et al.*, 2015; *Xue et al.*, 2014). The episodes in summer 2011 were attributed to fast photochemistry of $HNO_{3(g)}$ under ammonium rich conditions (*Griffith et al.*, 2015) and those in winter 2009 were assumed to be caused by hydrolysis of N_2O_5 (*Xue et al.*, 2014). To shed some light on this topic, an integrated field experiment was conducted in the present study measuring water-soluble inorganic ions, trace gases, particle size distribution and aerosol vertical backscatter density at high time resolution using online instruments at an urban site in Guangzhou of the PRD. In addition, vertical profiles of humidity, temperature, and wind speed and direction were obtained from the Guangzhou national weather station located 18.0 km northeast of the measurement site. Potential formation mechanisms for daytime nitrate episodes were explored through in-depth data analysis.

2. Methodology

2.1 Site description

The measurement site is located inside the South China Institute of Environmental Science (SCIES) (23°07′N, 113°21′E), which represents a typical urban environment in Guangzhou, south China (*Tao et al.*, 2012). The instruments were mounted on the roof of a building 50 m above ground and the data were

collected during 15 October to 6 November 2015.

2.2 Online measurements of water-soluble inorganic ions and gaseous precursors

Water-soluble inorganic ions (Na^+, NH_4^+, K^+, Mg^{2+}, Ca^{2+}, NO_2^-, SO_4^{2-}, NO_3^-, Cl^-, and F^-) and gaseous precursors (SO_2, HNO_3, NH_3, and HCl) were measured by an In-situ Gas and Aerosol Composition monitoring system (IGAC, Model S-611, Machine Shop, Fortelice International Co., Ltd., Taiwan, China) with an hourly temporal resolution (*Young et al.*, 2016). The IGAC consists of a wet annular denuder (WAD), a scrub and impact aerosol collector (SCI), and an ion chromatography (IC). Gases and aerosols were passed through WAD at a flow rate of 16.7 L min^{-1}, with a $PM_{2.5}$ cyclone. The WAD is made of two concentric Pyrex glass cylinders and set up vertically to the ground. The inner walls of the annulus are wetted with dilute H_2O_2 solution (5 mM in ultrapure water). At the inlet of the SCI, the opening of an L-shaped water-spray nozzle is located at the centerline of the air stream and faces upstream. Ultrapure water is fed continuously to the nozzle at 1.0 mL min^{-1} and heated to about 140 °C. Hot water steam is sprayed directly towards the particle-laden air to enhance mixing and particle-liquid contact. Then, aerosols are subjected to condensation growth in the remaining section of the SCI. The grown aerosols are accelerated through a conical-shaped impaction nozzle and collected on the impaction plate. At the base of the impaction plate, standard sample of LiBr solution is added continuously to the aerosol liquid sample at around 0.1 mL min^{-1}. The gas and aerosol liquid samples from the WAD and SCI are drawn separately by a pair of syringe pumps, between which one syringe collects the current sample (~50 min) and the other injects the previous sample. The samples are then subsequently and simultaneously analyzed for anions and cations by two IC systems.

Cations (Li^+, Na^+, NH_4^+, K^+, Mg^{2+} and Ca^{2+}) were measured by an IC system

(Dionex ICS-1100) using a CS12A column with 20 mM methanesulfonic acid eluent. Anions (F^-, Br^-, NO_2^-, SO_4^{2-}, NO_3^- and Cl^-) were measured by another IC system (Dionex ICS-2100) using an AS19 column with 20 mM KOH eluent. System blank values were subtracted from sample concentrations. Method detection limits of ions were within the range of 0.001 to 0.003 mg L^{-1}.

A know concentration of LiBr was used as internal standards by adding to the aerosol liquid samples to determine the stability of IGAC system. The changes of internal standards during the study period were within 8%. Eight concentration gradients of the mixed standard solutions containing the above-mentioned cations and anions (0.005, 0.01, 0.02, 0.05, 0.1, 0.2, 0.5 and 1.0 mg L^{-1}) were used to calibrate the IC systems' response with respect to analytic concentrations. The calibration curves for each ion were then obtained and used to quantify the ions concentrations of ambient samples. The IC systems were calibrated with above eight sets of mixed standard solutions once every four weeks. The uncertainties of the IC systems were generally less than 15% according to the calibration curves for each ion.

2.3 Online measurements of aerosol size

A Scanning Mobility Particle Sizer (SMPS; TSI Model 3936, TSI, Inc., St. Paul, MN) combined with a long Differential Mobility Analyzer (DMA; TSI Model 3080) and a Condensation Particle Counter (CPC; TSI Model 3010) was used to measure submicron particle size. The sample and sheath flows through the long DMA were 0.3 and 3.0 L min^{-1}, respectively. It allows particles to be classified into the range of 14 nm - 615 nm (D_{mob}, mobility diameter) with an inside impact inlet (nozzle size is 0.0457cm). A total of 167 bins (sizes) of particles were scanned and measured in 5 min. An Aerodynamics Particle Sizer (APS; TSI Model 3321) was used to measure the distributions of fine and coarse particle sizes. The sample and sheath flow rates of

APS were 1.0 and 4.0 L min^{-1}, respectively. A total of 52 bins (sizes) of particles in the range of 542 nm - 10 μm (D_a, aerodynamics diameter) were measured at 5 min resolution.

Ambient air first passed through two total suspended particulate (TSP) cyclones, then passed through two stainless steel tube and two Nafion driers (Perma Pure, Model MD-700-36S-1) prior to be measured by the SMPS and APS. The dry sweeping gas of two Nafion driers was produced by an air compressor pump. Two relative humidity sensors were set up in the links between Nafion driers, SMPS and APS. The relative humidity of sample flow was controlled to be below 30% by the flow rate of the dry sweeping gas.

2.4 Online measurements of vertical backscatter density

Vertical backscatter density was measured by a ceilometer (Vaisala Corp., Helsinki, Finland; Model CL-31) (*Munkel et al., 2007*). CL-31 is equipped with the InGaAs diode laser, which emits pulses at a wavelength of 910 nm. Backscattered vertical profile of aerosol signal was observed at a temporal resolution of 2 second and spatial resolution of 15 meter. The entire range of the signal is 5.0 km height in this study.

2.5 Online measurements of meteorological parameters

The ground meteorological parameters (e.g. wind direction and speed, relative humidity (RH), temperature, and precipitation) were measured every 10 min at an automatic meteorological station (Vaisala Company, Helsinki, Finland, model MAWS201), which was mounted on the roof of the SCIES site (53 m above ground). Vertical profiles of RH, temperature, and wind speed and direction were obtained from the Guangzhou national weather station (23°13′N, 113°29′E) located 18.0 km northeast of the SCIES site. Vertical profiles of RH and temperature were measured

by a high precision microwave radiometer (Radiometer Physics GmbH, RPG-HATPRO-G4, Meckenheim, Germany). The measurement range of the microwave radiometer was only up to 2000 meters height with 10-100 meters resolution. Vertical profiles of wind speed and direction were measured every 6-min by a wind profiler (Aerospace Science & Industry Corporation, CFL-16, China), which provided 25 levels of data below ~3 km with a vertical resolution of 120 m.

2.6 Data analysis

Liquid water content (LWC) shown in Fig. 1 was calculated using the ISORROPIA II thermodynamic equilibrium model for K^+–Ca^{2+}–Mg^{2+}–NH_4^+–Na^+–SO_4^{2-}–NO_3^-–Cl^-–H_2O aerosols. The input data included K^+, Ca^{2+}, Mg^{2+}, NH_4^+, Na^+, SO_4^{2-}, NO_3^-, Cl^-, $HNO_{3(g)}$, $NH_{3(g)}$, $HCl_{(g)}$, ambient RH and temperature on the ground, and the forward mode was used for the calculation (*Fountoukis and Nenes*, 2007). The uncertainties of the calculated LWC were estimated to be less than 20% according to the measurement uncertainties of the water-soluble inorganic ions, gaseous precursors, ambient RH and temperature.

To investigate the air mass origins of the pollutants arriving at SCIES, 24 h backward trajectories were calculated at an elevation of 500 m every hour during the daytime nitrate episodes on 27 and 28 October in 2015 using the HYbrid Single-Particle Lagrangian Integrated Trajectory (HYSPLIT) 4 model (http://ready.arl.noaa.gov/HYSPLIT.php).

3. Results and Discussion

3.1 Elevated nitrate episodes

The average concentrations of SO_4^{2-}, NO_3^- and NH_4^+ were 10.9±3.5, 4.9±6.5 and 3.9±2.8 μg m^{-3} during the study period, accounting for 49±10%, 16±10% and 15±4% of the total water-soluble inorganic ions (WSII) in $PM_{2.5}$, respectively (Table 1).

Although the concentration of NO_3^- was only half of that of SO_4^{2-} on campaign average, its hourly maximum was more than doubled that of SO_4^{2-}, suggesting the much large variations of NO_3^- than SO_4^{2-} in urban Guangzhou, as was seen from their standard deviations and the 10^{th}-90^{th} percentile values. To explore possible mechanisms causing the high nitrate concentration, nitrate episodes were first identified as cases with hourly NO_3^- concentration above the 90^{th} percentile (> 9.5 μg m^{-3}) and continued for more than five hours. A total of four episodes were identified with two occurred during daytime (on 27 and 28 October) and the other two during nighttime (on 15 and 16 October) (Fig. S1).

The average concentrations of NO_3^- were 17.9 μg m^{-3} and 30.6 μg m^{-3} during the daytime and nighttime episodes, respectively (Table 1). Compared with the non-episodes, NO_3^- was enhanced the most (by a factor of 5.1 and 8.7 during daytime and nighttime episodes, respectively), followed by NH_4^+ (a factor of 3.0 and 4.2) and SO_4^{2-} (a factor of 1.6 and 1.8). Their gaseous precursors (e.g. NH_3, SO_2, HNO_3, NOx) were only enhanced by a factor of 1.2-1.8 during the nitrate episodes. The somewhat more enhanced NH_4^+ than SO_4^{2-} was due to its association with NO_3^-. The enhancement rates of NO_3^- were much higher than those of SO_4^{2-}, especially during the nighttime episodes due to the hydrolysis of N_2O_5 (Fig.S2). As expected, the average ambient RH at ground level during the nighttime episodes was close to its 90^{th} percentile value. Although the average ambient temperature at ground level during the daytime episodes was equal to its 90^{th} percentile value, the average ambient RH was still much higher than its average and median values, suggesting the daytime episodes were likely related to aqueous-phase reactions.

Insert Table 1

3.2 Formation mechanisms for daytime elevated ambient nitrate

To shed some light on the possible formation mechanisms causing the daytime nitrate episodes, relevant parameters including deliquescence relative humidity (DRH), dissociation constant (K_p) of NH_4NO_3 and LWC of inorganic aerosols were calculated (Fig. 1). DRH and K_p, the reciprocal functions of ambient temperature, can be used to evaluate the thermodynamic properties of NH_4NO_3. When ambient RH > DRH, nitrate is prone to exist in aqueous phase, otherwise in solid phase (*Seinfeld & Pandis*, 2012). Nitrate in solid phase (NH_4NO_3) can dissociate to $HNO_{3(g)}$ and $NH_{3(g)}$ at high K_p value condition. The mole equivalent concentrations of NH_4^+, SO_4^{2-} and NO_3^- indicated that there was enough NH_4^+ to neutralize both SO_4^{2-} and NO_3^- (Fig. 2). Thus, NH_4NO_3 could exist in solid phase or in aqueous phase as NH_4^+ and NO_3^- according to the relationship between ambient RH and DRH.

Fig. 1 shows that the ambient RH was evidently lower than or equal to DRH and K_p was at high levels during the daytime episodes. NH_4NO_3 was thus expected to be existed in solid phase, and was prone to dissociate to NH_3 and HNO_3. Interestingly, NO_3^- concentration increased rather decreased with increasing K_p value. OH· was not measured in this study, but its diurnal variation was likely similar to that of O_3 and was generally at high concentration levels during the daytime in the PRD region (*Hofzumahaus et al.*, 2009). The concurrent increases of O_3 and NO_3^- raised the possibility of significant contribution of NO_2 oxidation via OH· to daytime nitrate episode. However, simultaneous increases of nitrate and its gaseous precursors (e.g. NO_2 and HNO_3) concentrations excluded such a possibility. Furthermore, NO_x concentrations were slightly lower during the episodes than the average values before or after the episodes. The paradox phenomena mentioned above indicated other

219 possibilities causing the daytime episodes.

220 Particle size distribution can provide some evidences on the formation
221 mechanisms of major inorganic ions in the atmosphere (*Yao et al.*, 2003; *Zhuang et al.*,
222 1999). The condensation mode particles can be considered from gas-phase reactions
223 while the droplet model from aqueous-phase processes (*John et al.*, 1990). As shown
224 in Fig. 3a and Fig. 3b, particle number concentration in droplet mode (aerodynamic
225 diameter ranged from 600 nm to 700 nm) evidently increased during the daytime
226 episodes while that of condensation mode (mobility diameter < 200 nm) changed little.
227 Aerodynamic diameters of condensation mode particles were estimated to be less than
228 300 nm based on their average density (about 1.5 g cm^{-3}) of the measured
229 size-resolved chemical components on 27 and 28 October. Thus, the daytime nitrate
230 episodes were likely from aqueous-phase processes rather than the gas-phase
231 reactions between NH_3 and HNO_3.

232

233 *Insert Fig. 1*

234 *Insert Fig. 2*

235 *Insert Fig. 3*

236

237 As expected, aerosol backscatter density near the ground showed a good
238 agreement with the timing of daytime episodes on 27 and 28 October (Fig. 4). Clouds
239 were identified at 500-1000 meters above the ground before daytime elevated nitrate
240 episodes. These clouds gradually disappeared afterwards due to strong solar radiation
241 causing cloud droplets evaporation. Aerosol particles produced from evaporated cloud
242 droplets can be vertically transported to the surface through turbulent mixing and
243 gravitational setting. For example, clouds appeared at about 750 meters above the

ground during 9:30-12:00 on 27 October (Fig. 4), dissipated afterwards, and accompanied with enhanced nitrate concentration during 12:00 to 16:00 on 27 October (the first daytime nitrate episode). The time evolution of the vertical distribution of aerosol backscatter density showed vertical diffusion of the cloud evaporation produced particles both downward and upward (Fig. 4). A similar pattern was also observed during the second daytime nitrate episode (on 28 October). It is likely that cloud processes played an important role causing daytime nitrate episodes.

Insert Fig. 4

3.3 Dynamics mechanisms of cloud processed aerosols

To further investigate the effective dynamics mechanisms of transporting cloud processed aerosols to surface-level during the daytime episodes, impact of regional transport should be first assessed. Horizontal wind speed and direction at different heights were plotted during the daytime nitrate episodes on 27 and 28 October (Fig. 5a and 5b). Here, east wind is defined as wind coming from the east and the same definition is used for other wind directions. Wind directions below the 1000 m height were from the northwest to northeast during the nitrate episode on 27 October and from the southeast during the nitrate episode on 28 October. Wind speeds at these levels were relatively weak (< 2 m s^{-1}). Similar wind directions were also obtained from air mass back trajectory analysis during these periods. For example, the weak wind from the northwest direction at 15:00 on 27 October and the strong wind from the southeast direction at 17:00 on 28 October were simulated by back trajectory analysis (Fig. 6a and 6b), which agreed with those observed by wind profiler at the height of 200 meters (Fig. 5a and 5b). During these daytime episodes, air masses

mainly originated from the southeast direction of Guangzhou with paths having few significant pollutant sources except urban Hong Kong (Zheng et al., 2009). In comparison, during another period (at 11:00 on 27 October, a few hours before the first episode) with no cloud evaporation but with air mass also passing over urban Hong Kong, much lower NO_3^- concentration was observed (Fig. 6a). Furthermore, the non-episode high NO_3^- concentrations were actually mainly associated with south and southwest wind directions (Fig. 7). Thus, the daytime nitrate episodes were not caused by regional transport of pollutants.

Insert Fig. 5

Insert Fig. 6

Insert Fig. 7

Clouds formed about 2-3 hours before the daytime nitrate episode were at the height just above the top of boundary layer and were shallow stratocumulus clouds with a cloud depth of about 170-230 meters, which can be evaporated under strong solar radiation after sunrise. An inversion layer at the cloud top might have existed, but this cannot be firmly confirmed with the data we have. This is because the cloud top during the daytime periods was higher than 1000 meter, likely in the range of 1000-2700 meters as shown in Figure 4, while the measurement range of the microwave radiometer only covered the height up to 2000 meter and with a very low resolution of 100 meter at upper levels. Thus, if the cloud top was higher than 2000 meter, or if the cloud top was in between 1000-2000 meter but the inversion layer was very thin, the instrument would not be able to detect such an inversion layer. Furthermore, it is also possible that the temperature profiles were different between

the measure site (SCIES station) and the weather station 18 km away.

Despite the potential inversion layer at the cloud top during the 27 and 28 October episode, no inversion was seen within the boundary layer (<2000 meters) (Fig. 8a), providing the needed meteorological conditions for transporting residual aerosols produced from cloud evaporation to the lower-levels through strong turbulent mixing. Strong turbulence was indeed observed during the daytime nitrate episodes with the vertical velocity up to 0.3 m s^{-1} at many levels below the original cloud base (Fig. 8b), enabling the residual aerosols to be able to transport the surface layer in just half to one hour. Furthermore, the transient high RH was simultaneously observed at all levels during the daytime episodes, further supporting the above hypothesis (Fig. 8c). It is also noticed that the duration was longer and the average nitrate concentration was higher on 28 October than 27 October episode, likely due to the stronger vertical turbulence (as seen from the observed vertical wind speed) on 28 October.

Insert Fig. 8

The average ratio of NO_3^-/SO_4^{2-} in ambient aerosols was 0.40±0.37 during the study period, which was within the range of the ratio (0.3-0.6) in precipitation in China during 2001-2015 (*Itahashi et al.*, 2017). However, the daytime nitrate episodes showed a much higher NO_3^-/SO_4^{2-} ratio (1.05), which was likely due to recycling of cloud condensation nuclei with each cycle having added nitrate. Furthermore, the moist condition in cloud was in favor of the reserve of NO_3^- in aqueous phase and prevented it from dissociating into $HNO_{3(g)}$ and $NH_{3(g)}$. In conclusion, vertical turbulent mixing of the residual aerosols produced from cloud evaporation well

explained the daytime episodes and the high concentrations of the droplet mode particles.

4. Summary and Implication

Differing from existing studies which frequently attributed high surface-level aerosol concentrations to enhanced source emissions and secondary aerosol formation, the present study identified a potentially important mechanism causing high nitrate concentration during daytime in the PRD. A conceptual framework is firstly needed for designing and simulating the cloud process in order to quantify its impact on nitrate concentration budget on seasonal and annual time scales. This framework should include aerosol-cloud interaction, gas- and aqueous-phase chemistry involving NH_4^+, SO_4^{2-} and NO_3^- particles, and more importantly, cloud evaporation releasing processed aerosols which can provide a pathway reasonably explaining daytime nitrate episodes in cloudy regions such as the PRD. Existing size- and chemically-resolved cloud microphysics models such as the one described in *Zhang et al.* (2006) can be modified for conducting such modeling studies.

This study suggested that SO_4^{2-} and NO_3^- were mostly fully neutralized by NH_4^+ in the PRD. In this scenario NO_3^- formed in cloud water would combine with NH_4^+ or react with NH_3 to form NH_4NO_3 in solid phase, rather than dissociate to HNO_3 during cloud evaporation process. With further reduced SO_2 emission in many parts of China, the contribution of nitrate to fine particles become more important in ammonia rich conditions. In the PRD, emissions of NO_x from industry have declined while those from traffic have slightly increased due to the increase of the number of vehicles (*Zheng et al.*, 2009). Little attention has been paid on NH_3 emission in the PRD as well as other parts of China. Emission reduction of both NO_x and NH_3 should be considered together for reducing fine particles.

Acknowledgments

This study was supported by the National Natural Science Foundation of China (No.41475119 and 41603119) and the Central Research Institute's Basic Scientific Special Funds (No. PM-ZX703-201602-053).

References

Alexander, B., Hastings, M. G., Allman, D. J., Dachs, J., Thornton, J. A., & Kunasek, S. A. (2009). Quantifying atmospheric nitrate formation pathways based on a global model of the oxygen isotopic composition ($\Delta^{17}O$) of atmospheric nitrate. *Atmospheric Chemistry and Physics*, *9*(14), 5043-5056. https://doi.org/10.5194/acp-9-5043-2009

Andreae, M. O., & Merlet, P. (2001). Emission of trace gases and aerosols from biomass burning. *Global Biogeochemical Cycles*, *15*(4), 955-966. https://doi.org/10.1029/2000GB001382

Chang, W. L., Bhave, P. V., Brown, S. S., Riemer, N., Stutz, J., & Dabdub, D. (2011). Heterogeneous atmospheric chemistry, ambient measurements, and model calculations of N_2O_5: A review. *Aerosol Science and Technology*, *45*(6), 665-695. http://dx.doi.org/10.1080/02786826.2010.551672

Dall'Osto, M., Harrison, R. M., Coe, H., Williams, P. I., & Allan, J. D. (2009). Real time chemical characterization of local and regional nitrate aerosols. *Atmospheric Chemistry and Physics*, *9*(11), 3709-3720. https://doi.org/10.5194/acp-9-3709-2009

Davidson, E. A. F., & Kingerlee, W. (1997). A global inventory of nitric oxide emissions from soils, *Nutrient Cycling in Agroecosystems*, 48, 37-50. https://doi.org/10.1023/A:1009738715891

Fountoukis, C., & Nenes, A. (2007), ISORROPIA II: a computationally efficient thermodynamic equilibrium model for K^+–Ca^{2+}–Mg^{2+}–NH_4^+–Na^+–SO_4^{2-}–NO_3^-–Cl^-–H_2O aerosols, *Atmospheric Chemistry and Physics*, *7*(17), 4639-4659. https://doi.org/10.5194/acp-7-4639-2007

Griffith, S. M., Huang, X. H. H., Louie, P. K. K., & Yu, J. Z. (2015). Characterizing the thermodynamic and chemical composition factors controlling $PM_{2.5}$ nitrate: Insights gained from two years of online measurements in Hong Kong. *Atmospheric Environment*, *122*, 864-875, http://dx.doi.org/10.1016/j.atmosenv.2015.02.009

Hofzumahaus, A., Rohrer, F., Lu, K., Bohn, B., Brauers, T., Chang, C., … Zhang, Y. (2009). Amplified trace gas removal in the troposphere. *Science*, *324*(5935), 1702-1704. https://doi.org/10.1126/science.1164566

Hudman, R. C., Jacob, D. J., Turquety, S., Leibensperger, E. M., Murray, L. T., Wu, S., … Brune, W. H. (2007). Surface and lightning sources of nitrogen oxides over the United States: Magnitudes, chemical evolution, and outflow. *Journal of Geophysical Research*, *112*, D12S05. https://doi.org/10.1029/2006JD007912

Itahashi, S., Yumimoto, K., Uno, I., Hayami, H., Fujita, S. I., Pan, Y., & Wang, Y. (2017). A 15-year record (2001-2015) of the ratio of nitrate to non-seasalt sulfate in precipitation over East Asia. *Atmospheric Chemistry and Physics Discussion*, 1-30, https://doi.org/10.5194/acp-2017-848.

John, W., Wall, S. M., Ondo, J. L., & Winklmayr, W. (1990). Modes in the size distributions of atmospheric inorganic aerosol. *Atmospheric Environment*, *24*(9), 2349-2359. https://doi.org/10.1016/0960-1686(90)90327-J

Munkel, C., Eresmaa, N., Rasanen, J., & Karppinen, A. (2007). Retrieval of mixing height and dust concentration with lidar ceilometer. *Boundary-Layer Meteorology*, *124*(1), 117-128. https://doi.org/10.1007/s10546-006-9103-3

Pathak, R. K., Wang, T., & Wu, W. S. (2011). Nighttime enhancement of $PM_{2.5}$ nitrate in ammonia-poor atmospheric conditions in Beijing and Shanghai: Plausible contributions of heterogeneous hydrolysis of N_2O_5 and HNO_3 partitioning. *Atmospheric Environment*, *45*(5), 1183-1191. https://doi.org/10.1016/j.atmosenv.2010.09.003

Richter, A., Burrows, J. P., Nus, H., Granier, C., & Niemeier, U. (2005). Increase in tropospheric nitrogen dioxide over China observed from space. *Nature*, *437*(7055), 129-132. https://doi.org/10.1038/nature04092

Seinfeld, J. H., & Pandis, S. N. (2012). *Atmospheric chemistry and physics: from air pollution to climate change*, John Wiley & Sons.

Shindell, D. T., Faluvegi, G., Koch, D., Schmidt, G. A., Unger, N., & Bauer, S. E. (2009). Improved attribution of climate forcing to emissions. *Science*, *326*(5953), 716-718. https://doi.org/10.1126/science.1174760

Stutz, J., Wong, K. W., Lawrence, L. E., Ziemba, L. D., Flynn, J., Rappengluck, B., & Lefer, B. L. (2010). Nocturnal NO_3 radical chemistry in Houston, TX. *Atmospheric Environment*, *44*(33), 4099-4106. https://doi.org/10.1016/j.atmosenv.2009.03.004

Tao, J., Shen, Z., Zhu, C., Yue, J., Cao, J., Liu, S., Zhu, L., & Zhang, R. (2012). Seasonal variations and chemical characteristics of sub-micrometer particles (PM_1) in Guangzhou, China, *Atmospheric Research*, *118*, 222-231. https://doi.org/10.1016/j.atmosres.2012.06.025

Tao, J., Zhang, L., Cao, J., & Zhang, R. (2017). A review of current knowledge concerning $PM_{2.5}$ chemical composition, aerosol optical properties and their relationships across China, *Atmospheric Chemistry and Physics*, *17*(15), 9485-9518. https://doi.org/10.5194/acp-17-9485-2017.

Wängberg, I., Etzkorn, T., Barnes, I., Platt, U., & Becker, K. H. (1997). Absolute determination of the temperature behavior of the $NO_2 + NO_3 + (M) \leftrightarrow N_2O_5 + (M)$ equilibrium. *The Journal of Physical Chemistry A*, *101*(50), 9694-9698. https://doi.org/10.1021/jp972203o.

Wang, H., Lu, K., Chen, X., Zhu, Q., Chen, Q., Guo, S., … Zhang, Y. (2017). High N_2O_5 concentrations observed in urban Beijing: Implications of a large nitrate formation pathway, *Environmental Science & Technology Letters*, *4*(10), 416-420, https://doi.org/10.1021/acs.estlett.7b00341.

Wang, X., Zhang, Y., Chen, H., Yang, X., Chen, J., & Geng, F. (2009). Particulate nitrate formation in a highly polluted urban area: A case study by single-particle mass spectrometry in Shanghai. *Environmental Science & Technology*, *43*(9), 3061-3066. https://doi.org/10.1021/es8020155

Watson, J. G. (2002). Visibility: Science and regulation. *Journal of the Air & Waste Management Association*, *52*(6), 628-713. http://dx.doi.org/10.1080/10473289.2002.10470813

Wen, L., Chen, J., Yang, L., Wang, X., Xu, C., Sui, X., … Zhu, T. (2015). Enhanced formation of fine particulate nitrate at a rural site on the North China Plain in summer: The important roles of ammonia and ozone. *Atmospheric Environment*, *101*, 294-302. https://doi.org/10.1016/j.atmosenv.2014.11.037

Xue, J., Yuan, Z., Lau, A. K. H., & Yu, J. Z. (2014). Insights into factors affecting nitrate in $PM_{2.5}$ in a polluted high NOx environment through hourly observations and size distribution measurements. *Journal of Geophysical Research*, *119*(8), 4888-4902. https://doi.org/10.1002/2013JD021108

Yao, X., Lau, A. P. S., Fang, M., Chan, C. K., & Hu, M. (2003). Size distributions and formation of ionic species in atmospheric particulate pollutants in Beijing, China: 1-inorganic ions. *Atmospheric Environment*, *37*(21), 2991-3000. https://doi.org/10.1016/S1352-2310(03)00255-3

Young, L., Li, C., Lin, M., Hwang, B., Hsu, H., Chen, Y., …Tsai, P. (2016). Field performance of a semi-continuous monitor for ambient $PM_{2.5}$ water-soluble inorganic ions and gases at a suburban site. *Atmospheric Environment*, *144*, 376-388. http://dx.doi.org/10.1016/j.atmosenv.2016.08.062

Zhang, L., Michelangeli, D. V., Djouad, R., & Taylor, P. A. (2006). Modeling studies of the sulfur cycle in low-level, warm stratiform clouds. *Atmospheric Research*, *80*(2), 187-217. https://doi.org/10.1016/j.atmosres.2005.08.001.

Zhang, Q., Jimenez, J. L., Canagaratna, M. R., Allan, J. D., Coe, H., Ulbrich, I. M., … Worsnop, D. R. (2007). Ubiquity and dominance of oxygenated species in organic aerosols in anthropogenically-influenced Northern Hemisphere midlatitudes. *Geophysical Research Letters*, *34*(13). https://doi.org/10.1029/2007GL029979

Zhang, R., Wang, G., Guo, S., Zamora, M. L., Ying, Q., Lin, Y., … Wang, Y. (2015). Formation of urban fine particulate matter. *Chemical reviews*, *115*(10), 3803-3855. https://doi.org/10.1021/acs.chemrev.5b00067

Zheng, J., Zhang, L., Che, W., Zheng, Z., & Yin, S. (2009). A highly resolved temporal and spatial air pollutant emission inventory for the Pearl River Delta region, China and its uncertainty assessment. *Atmospheric Environment*, *43*(32), 5112-5122. https://doi.org/10.1016/j.atmosenv.2009.04.060

Zhuang, H., Chan, C. K., Fang, M., & Wexler, A. S. (1999). Size distributions of particulate sulfate, nitrate, and ammonium at a coastal site in Hong Kong. *Atmospheric Environment*, *33*(6), 843-853. https://doi.org/10.1016/S1352-2310(98)00305-7

Table 1 Statistics of hourly mass concentrations of water-soluble inorganic ions in $PM_{2.5}$, trace gases and selected meteorological factors in urban Guangzhou, PRD.

	Average ±standard deviation	Minimum	10th	median	90th	Maximum	Daytime episode	Daytime non-episode	Nighttime episode	Nighttime non-episode
NH_4^+/μg m^{-3}	3.9±2.8	<0.1	1.6	3.3	6.9	18.8	10.2	3.4	13.3	3.2
Na^+/μg m^{-3}	0.6±0.2	0.4	0.5	0.6	0.8	1.7	0.8	0.6	0.7	0.6
K^+/μg m^{-3}	2.0±0.3	1.5	1.6	1.9	2.4	3.6	2.0	2.0	3.2	2.0
Mg^{2+}/μg m^{-3}	0.2±0.0	0.2	0.2	0.2	0.2	0.3	0.2	0.2	0.2	0.2
Ca^{2+}/μg m^{-3}	0.1±0.1	0.0	0.0	0.1	0.2	0.7	0.1	0.1	0.1	0.1
SO_4^{2-}/μg m^{-3}	10.9±3.5	1.8	7.0	10.7	15.3	21.2	17.1	10.8	18.6	10.1
NO_3^-/μg m^{-3}	4.9±6.5	0.3	1.0	2.5	9.5	51.5	17.9	3.5	30.6	3.5
Cl^-/μg m^{-3}	0.6±0.6	0.0	0.2	0.4	1.4	5.6	1.2	0.5	1.7	0.5
NO_2^-/μg m^{-3}	0.8±0.4	0.0	0.3	0.7	1.2	2.8	1.0	0.6	1.6	0.8
WSII/μg m^{-3}	24.0±12.7	4.8	14.1	21.6	35.1	100.3	50.6	22.0	70.0	21.0
NH_3/μg m^{-3}	9.3±3.8	3.3	4.7	8.7	14.8	19.9	15.4	9.4	10.4	8.6
SO_2/μg m^{-3}	11.5±4.5	3.5	6.2	11.1	16.8	26.8	17.9	11.8	14.9	10.7
HNO_3/μg m^{-3}	1.7±0.7	0.5	1.0	1.5	2.7	5.0	3.5	1.9	2.0	1.4
NO/μg m^{-3}	16±27	<1	1	5	44	263	10	12	41	18
NO_2/μg m^{-3}	71±35	12	33	66	122	179	84	57	109	82
NO_x/μg m^{-3}	87±54	12	35	72	155	442	94	69	150	100
HCl/μg m^{-3}	0.1±0.2	0.0	0.0	0.0	0.3	0.8	0.4	0.2	0.0	0.0
HNO_2/μg m^{-3}	3.6±2.6	0.5	1.2	2.8	7.3	13.7	3.7	2.5	8.2	1.4
O_3/μg m^{-3}	53±52	1	3	31	134	252	114	81	46	23
RH/%	53±14	26	34	54	70	76	59	48	67	57
Temp/°C	25±3	16	21	26	29	31	29	26	25	24
WS/m s^{-1}	1.8±1.2	0.0	0.3	1.8	3.4	5.3	1.6	2.0	0.7	1.8

WSII: water-soluble inorganic ions; RH: relative humidity; Temp: temperature; WS: wind speed; daytime: 7:00-18:00; nighttime: 19:00-6:00

List of Figures

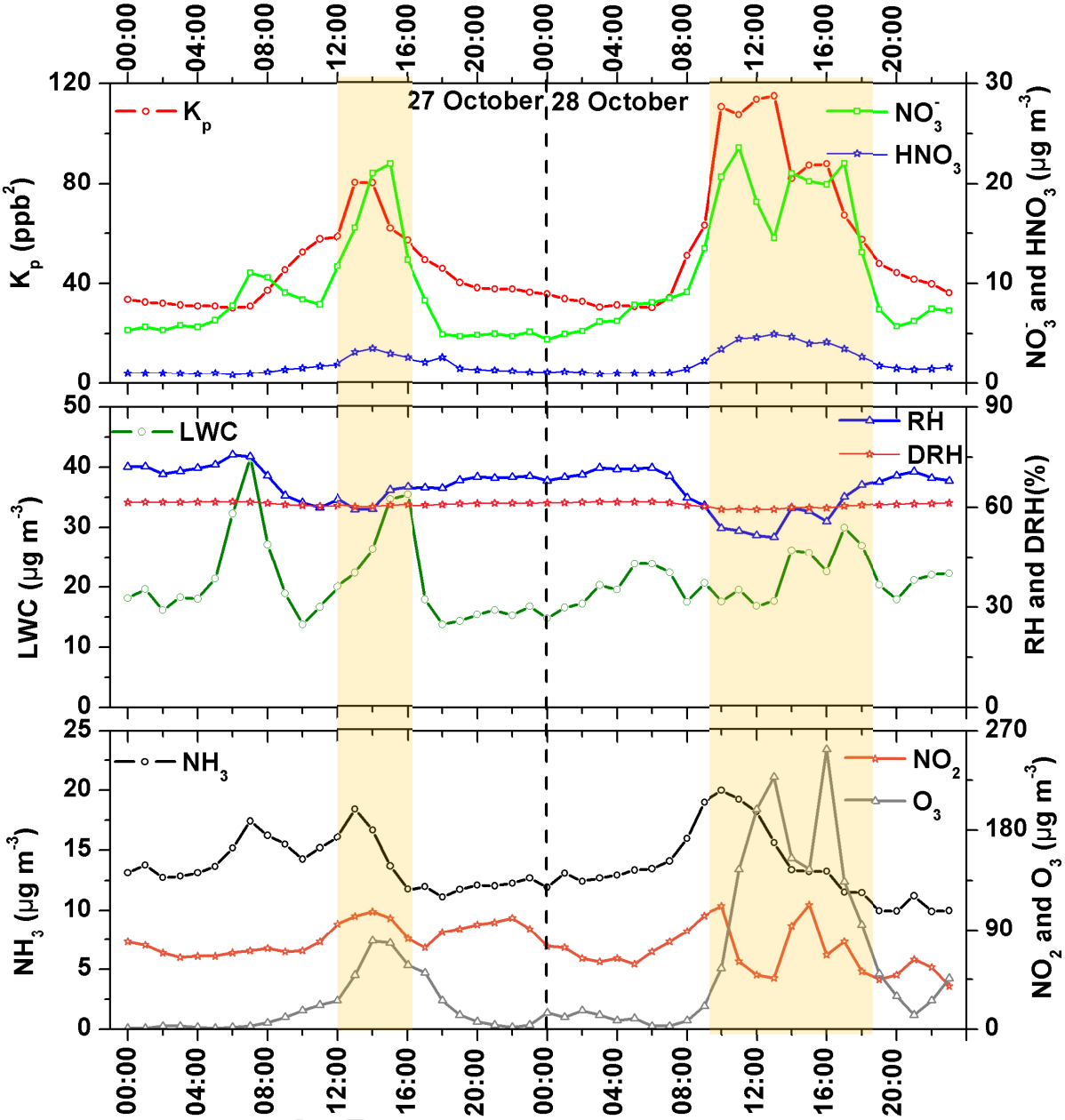

Fig. 1.

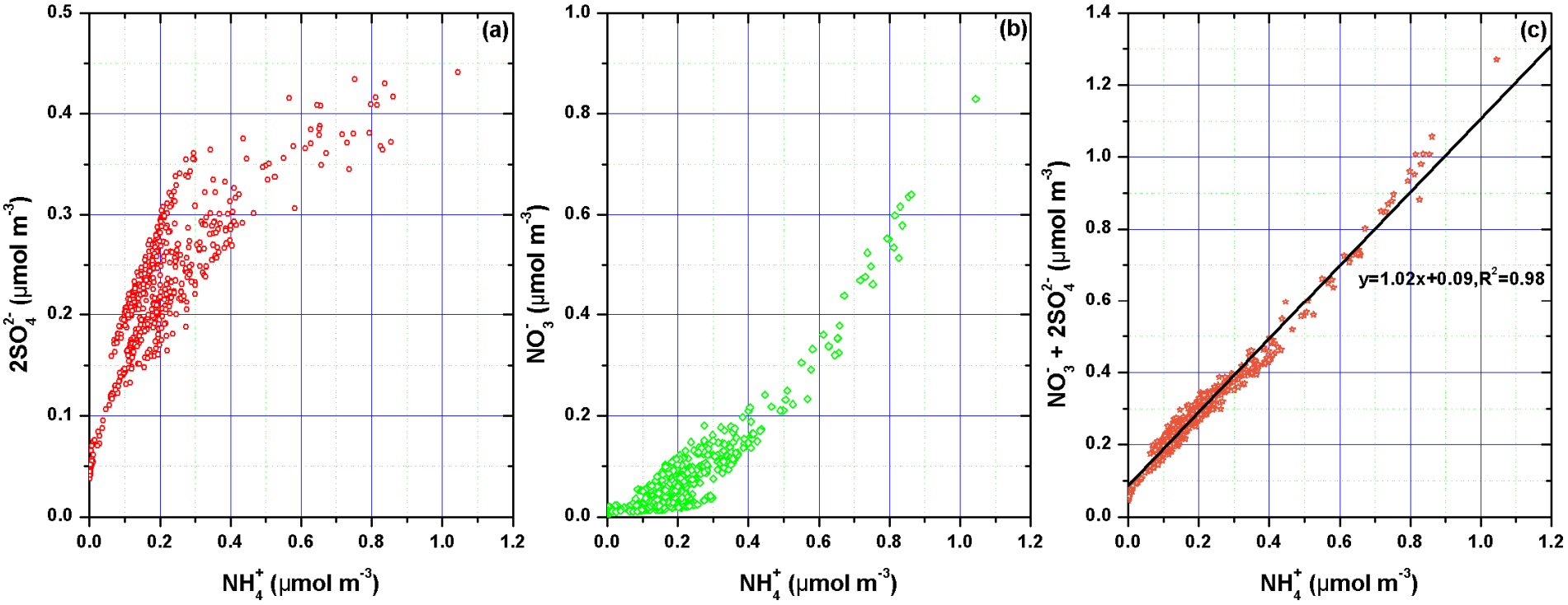

Fig. 2.

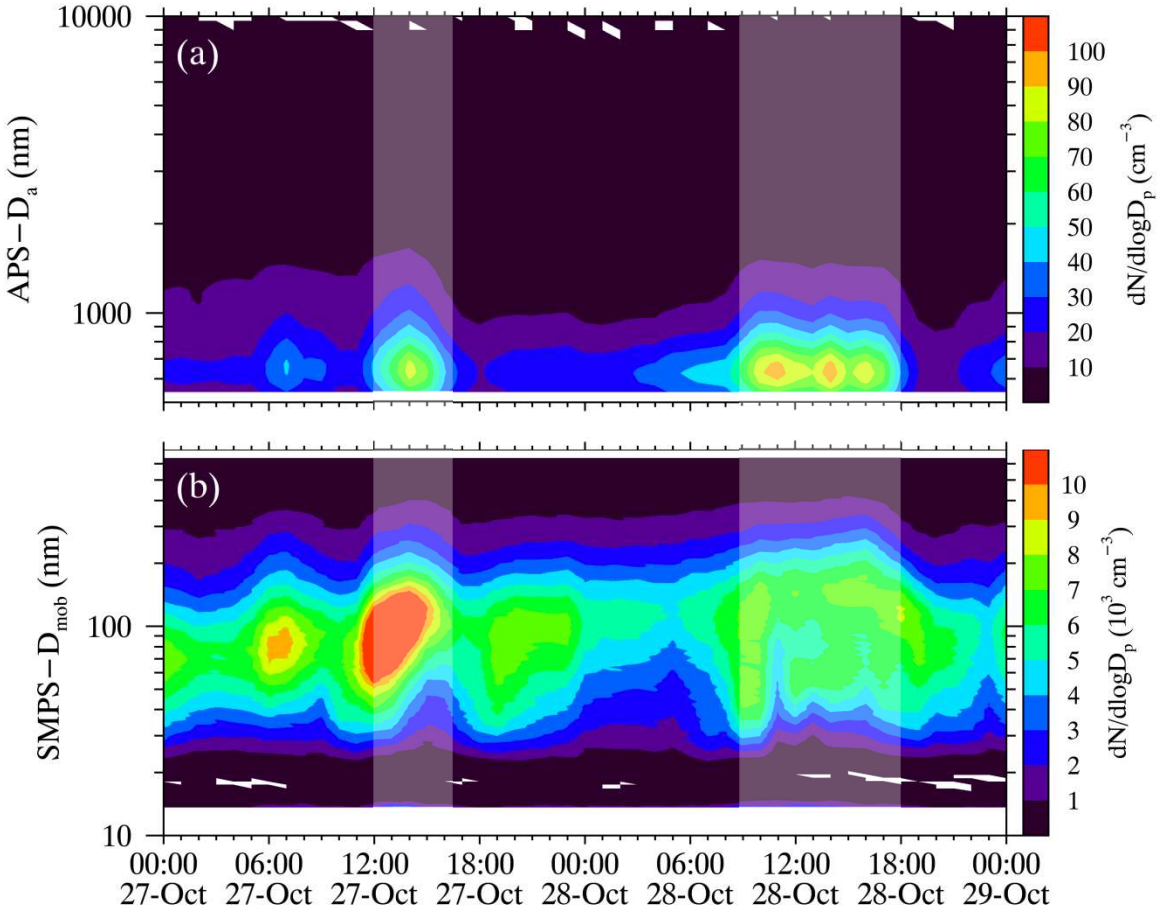

Fig. 3.

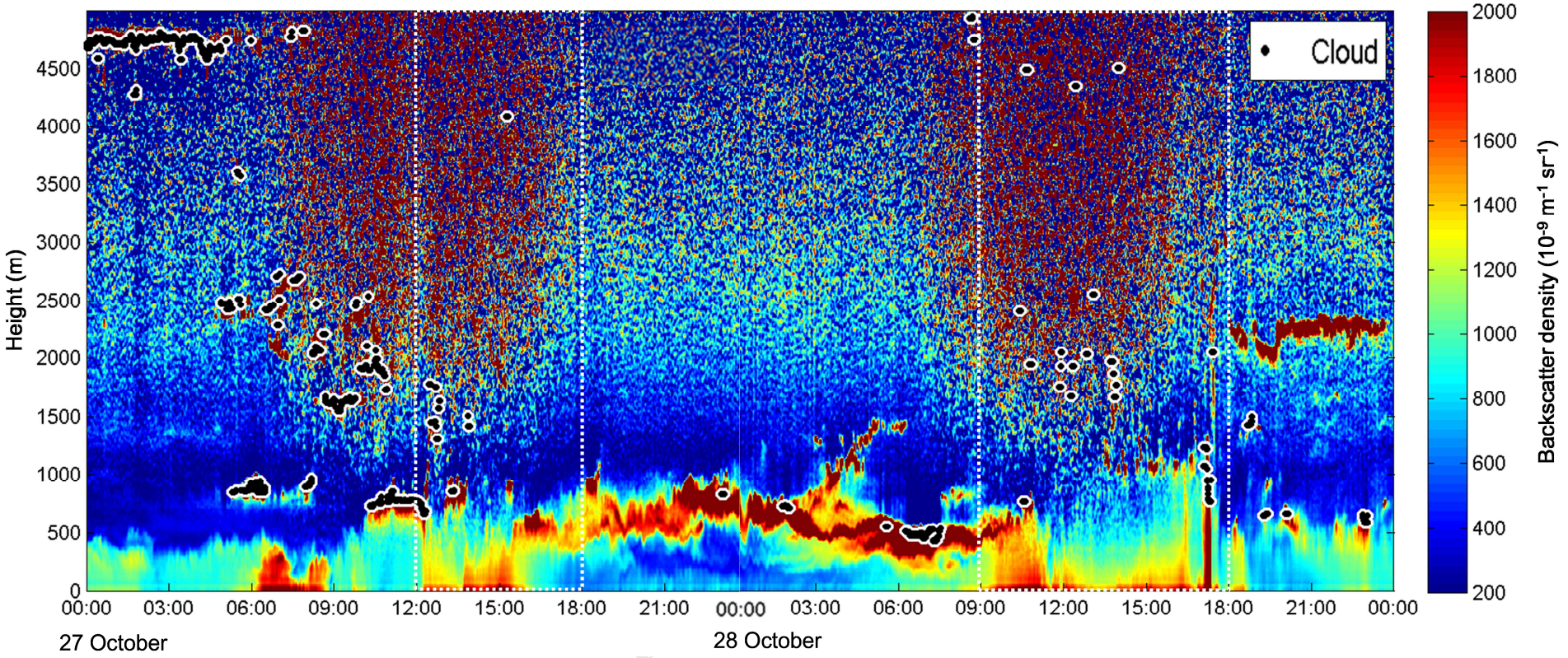

Fig. 4.

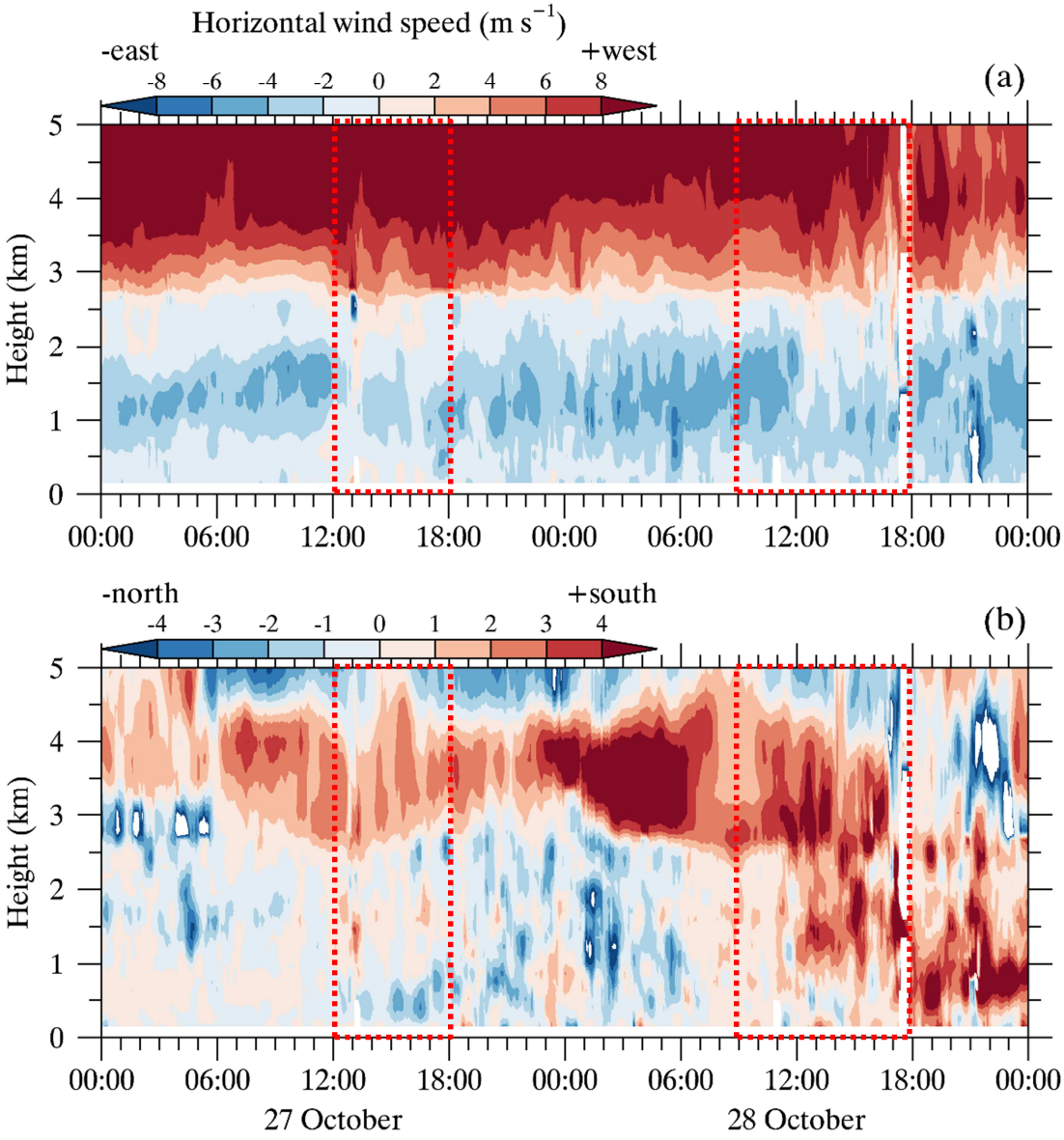

Fig. 5.

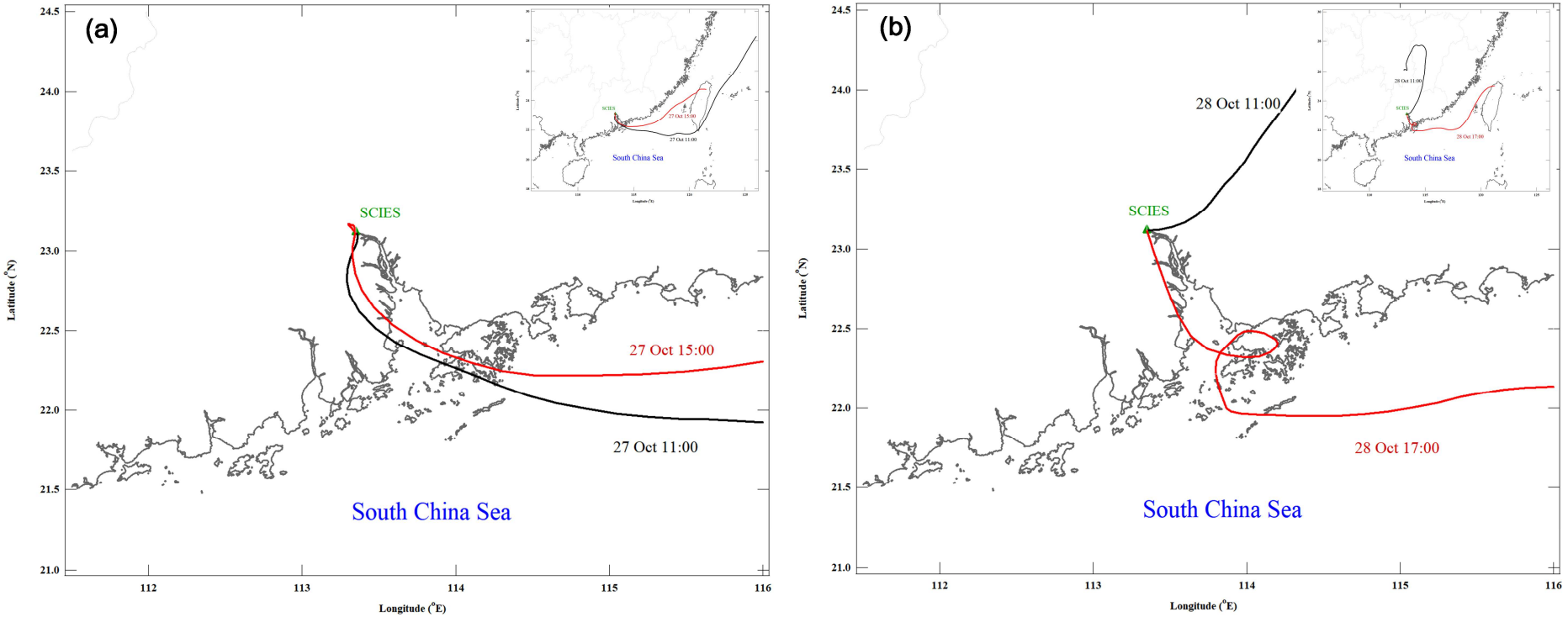
(a)
SCIES
27 Oct 15:00
27 Oct 11:00
South China Sea
Latitude (°N)
Longitude (°E)
(b)
28 Oct 11:00
SCIES
28 Oct 17:00
South China Sea
Latitude (°N)
Longitude (°E)

Fig. 6.

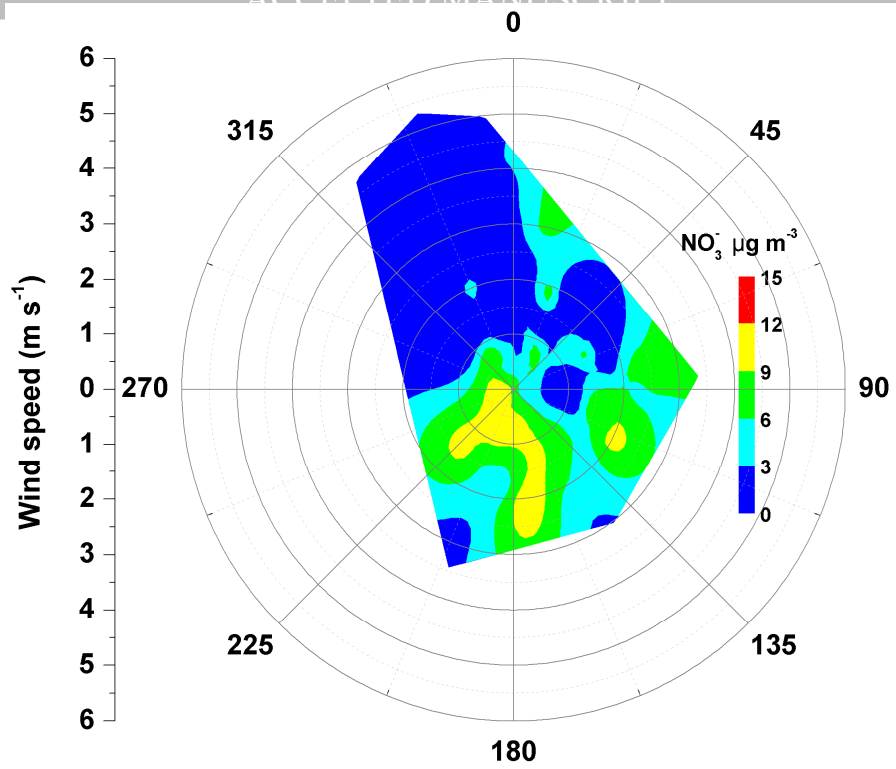

Fig. 7.

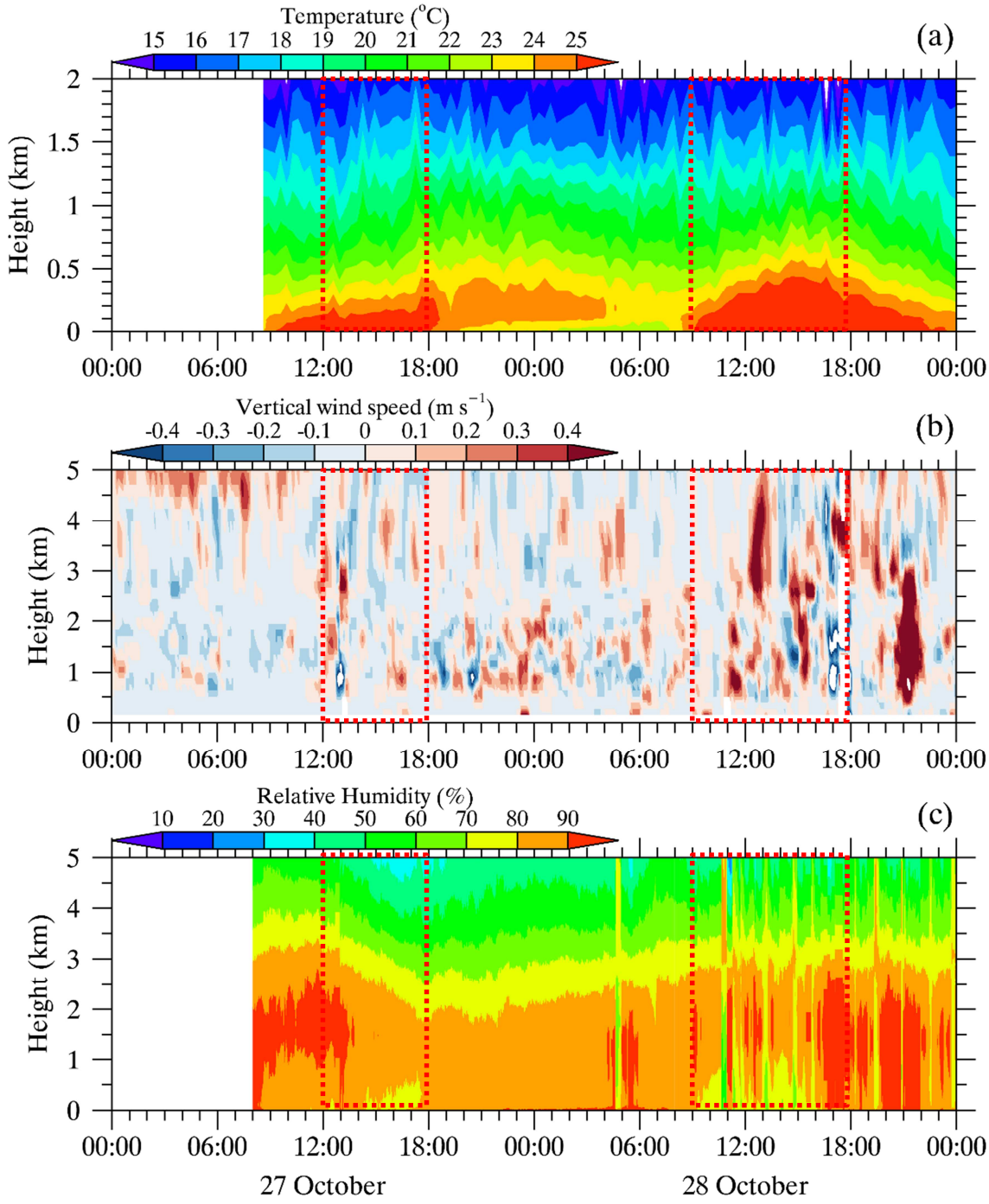
Temperature (°C)
15 16 17 18 19 20 21 22 23 24 25
(a)
Height (km)
2
1.5
1
0.5
0
00:00 06:00 12:00 18:00 00:00 06:00 12:00 18:00 00:00
Vertical wind speed (m s⁻¹)
-0.4 -0.3 -0.2 -0.1 0 0.1 0.2 0.3 0.4
(b)
Height (km)
5
4
3
2
1
0
00:00 06:00 12:00 18:00 00:00 06:00 12:00 18:00 00:00
Relative Humidity (%)
10 20 30 40 50 60 70 80 90
(c)
Height (km)
5
4
3
2
1
0
00:00 06:00 12:00 18:00 00:00 06:00 12:00 18:00 00:00
27 October
28 October

Fig. 8.

Highlights:

- $PM_{2.5}$ chemical composition and size distribution were measured
- Day- and nighttime nitrate episodes were observed
- Formation mechanisms causing daytime nitrate episodes were explored in detail
- Turbulent mixing of cloud processed aerosols caused daytime nitrate episodes